Article

Stochastic Dynamic Mass Spectrometric Quantitative and Structural Analyses of Pharmaceutics and Biocides in Biota and Sewage Sludge

Bojidarka Ivanova

Lehrstuhl für Analytische Chemie, Institut für Umweltforschung, Fakultät für Chemie und Chemische Biologie, Universität Dortmund, Otto-Hahn-Straße 6, 44221 Dortmund, Nordrhein-Westfalen, Germany; _ivanova@web.de or bojidarka.ivanova@yahoo.com

Abstract: Mass spectrometric innovations in analytical instrumentation tend to be accompanied by the development of a data-processing methodology, expecting to gain molecular-level insights into real-life objects. Qualitative and semi-quantitative methods have been replaced routinely by precise, accurate, selective, and sensitive quantitative ones. Currently, mass spectrometric 3D molecular structural methods are attractive. As an attempt to establish a reliable link between quantitative and 3D structural analyses, there has been developed an innovative formula $[D_{SD}^{'',tot} = \sum_i^n D_{SD}^{'',i} = \sum_i^n 2.6388.10^{-17} \times \overline{I_i^2} - (\overline{I_i})^2]$ capable of the exact determination of the analyte amount and its 3D structure. It processed, herein, ultra-high resolution mass spectrometric variables of paracetamol, atenolol, propranolol, and benzalkonium chlorides in biota, using mussel tissue and sewage sludge. Quantum chemistry and chemometrics were also used. Results: Data on mixtures of antibiotics and surfactants in biota and the linear dynamic range of concentrations 2–80 ng.(mL)$^{-1}$ and collision energy CE = 5–60 V are provided. Quantitative analysis of surfactants in biota via calibration equation $\ln[D''_{SD}] = f$(conc.) yields the exact parameter $|r| = 0.9999_1$, examining the peaks of BAC-C12 at m/z 212.209 ± 0.1 and 211.75 ± 0.15 for tautomers of fragmentation ions. Exact parameter $|r| = 1$ has been obtained, correlating the theory and experiments in determining the 3D molecular structures of ions of paracetamol at m/z 152, 158, 174, 301, and 325 in biota.

Keywords: mass spectrometry; stochastic dynamics; surfactants; biota; sludge; quantitative and 3D structural analyses

1. Introduction

Biocides and antibiotics are major classes of chemicals used to control or prevent the growth of microorganisms such as fungi, mosses, bacteria, lichens, and algae [1–3]. The therapeutics are efficacious at low concentration levels, due to specific interactions with single cellular targets. Conversely, biocides adsorb on a microbe's surface or are utilized for suspension at higher concentration levels compared with their minimum inhibitory concentrations. Their monitoring in the aquatic environment is of primary and increasing concern as well [4]. The main biocidal disposal route is via sewage systems and drains. The potential risk for bioaccumulation carries toxicological effects on the ecosystem [1,5–8]. The major chemical compositions of cleaning substances, including disinfectants, cosmetics, and personal care products, are surfactants [9–12]. Surfactants can be found in paints, polymer materials, fabrics, pesticides, and pharmaceutical products, in addition to oil, mining, and cellulose factories. They are emerging contaminants according to UNESCO [13]. The monitoring of the environmental and wastewater pollution of surfactants is a primary research task. Quaternary ammonium surfactants or so-called quats are toxic to aquatic organisms at a level of concentration of 1 mg.L^{-1} [1,14,15]. However, quaternary ammonium surfactants are not only toxic to environmental organisms, but also exhibit the

proliferation of antibiotic resistance [16]. In 2019, there were 4.95 million antibiotic-resistant pathogens around the world, which has been considered as a silent pandemic [10]. The therapeutics' abuse is a factor contributing to antibiotic resistance. It remains not well understood, but is recognized to be among the most pressing global environmental and human health problems [17,18]. It has been found that by 2050, approximately ten million people shall die, annually, as a result of antibiotic resistance [19]. Despite this, many quats play a vital role in biochemical pathways [20]. Benzalkonium chlorides (Figure 1) belong to the group of quaternary ammonium surfactants, and are extensively utilized for various industrial and domestic purposes [10,21,22], including contact lens solutions or eye drops [23–25]. For this reason, BAC-C14 is the most frequently detected biocide among benzalkonium chlorides in engineered and environmental systems [16]. Their presence in wastewater upset has led to activated sludge processes [26,27]. Benzalkonium chloride derivatives in sludge are capable of biodegrading during biological wastewater treatment or adsorbing onto a biomass. Their biodegradation paths have been examined [28–30]. The presence of benzalkonium chloride disinfectants in the environment promotes the abundance and diversity of antibiotic resistance genes in sewage sludge microbiomes [10]. Antibiotics, as surfactants and environmental pollutants, represent a widespread concern and ecotoxicological risk [23–25,31,32].
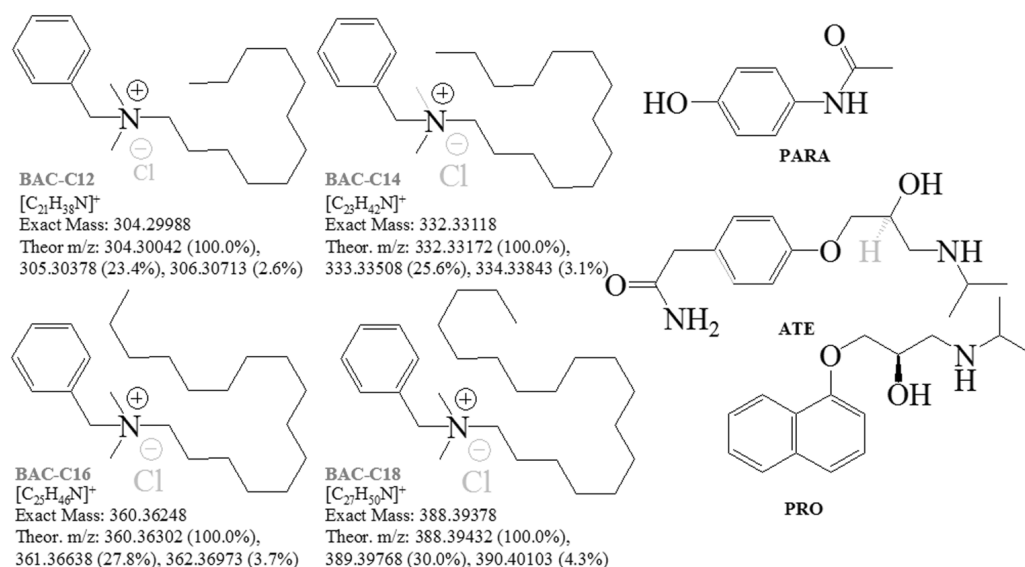
Figure 1. Chemical diagrams of benzalkonium chlorides and pharmaceutics; exact masses' theoretical m/z data in cationic form [M]⁺; theoretical mass spectrometric isotopic compositions and intensity ratios of the isotope shapes.

Atenolol and propranolol are *β*-blockers treating cardiovascular diseases [33]. They are emerging pollutants, found in sewage effluents and surface water. *Beta*-adrenergic receptors, which are major target macromolecules of *beta*-blockers, were detected in aquatic animals and fish. There is an environmental effect of the pharmaceutics on physiological processes in wild animals. The same can be said for paracetamol (tylenol or acetaminophen), which is a commonly used anti-inflammatory, antipyretic, and analgesic medication [32,34,35]. It can be found in tap water from the pharmaceutical industry and in urban and hospital waste [36]. There have been developed innovative strategies for the regulation of pharmaceutics in surface and groundwater via European legislation (Directives 2000/60/EC, 2008/105/EC, 2009/90/EC, 2013/39/EU, and 2015/1787/EU [37]).

The determination of pharmaceutics and biocides in biota, including the analysis of invertebrates, plankton, fish, human tissues and fluids, birds, and marine mammals, is importance for assessing the risk for human health and environmental damage [38,39], as well as determining the potential *ecological risk index* [38–40]. The *biomonitoring* includes

saltwater and freshwater mussels [1,41–43]. These biological species filter large quantities of water, thus accumulating both organic and inorganic pollutants from water or suspended matter at elevated levels. In addition, mussels are (i) widely distributed in the environment; (ii) sessile biological species; (iii) thrive in highly polluted areas; and (iv) easily sampled [41]. The biomonitoring of pollutants via mussels allows us (a) to determine the concentration levels of pollutants in feral organisms; (b) to examine the spatial (geographic) distribution of pollution, if any; and (c) to study the temporal distribution and variation of pollution toward distinct seasons. The *toxicokinetics* examines four major processes of biological objects such as mussels, involving (a) the adsorption of pollutants; (b) their distribution, (c) metabolism, and (d) excretion [44]. The rates of the processes determine the *contaminant's bioavailability*. Knowledge of the adsorption capability of pollutants is of importance, because the process is also used to decontaminate water. It plays a crucial role in methods for the removal of organics in wastewater treatment plants, thus highlighting the aerobic and anaerobic sludge systems [45,46]. The importance of the development of methods for determining surfactants and antibiotics in mixtures in biological and environmental samples is due to the fact that benzalkonium chlorides, for example, are used in commercial pharmaceutical formulations [47]. Catanionic mixtures of drug-surfactant aggregates such as benzalconium chlorides and β-blockers such as alprenolol, ATE, and PRO have been detailed [21,22]. β-Blockers have been used to treat ocular hypertension and glaucoma. Their pharmaceutical formulations with benzalconium chlorides have been examined in skin creams or eye drops [48].

Routinely, MS methods have been used to determine organic pollutants [1,49,50]. The ultra-high resolving power, selectivity, accuracy, precision, and sensitivity of tandem mass spectrometry are irreplaceable, being used for the analysis of environmental and biological samples. However, MS cannot be used as a universal method for determining mixtures of quaternary ammonium derivatives simultaneously [5,6,27,51].

Analytical mass spectrometry is a complex term, referring to three major research tasks of *qualitative*, *quantitative*, and *structural analyses*. However, pursuing the exact *chemometrics* (|r| = 1) is a challenging analytical task [52–58]. Among theoretical model equations that are particularly relevant are those producing exact method performance. Accordingly, research effort has been devoted to developing MS methods for data processing, ensuring the quality and comparability of analytical information toward the interpretation of results [59], which is in agreement with Council Directives 96/23/EC and 2002/657/EC.

However, depending on the analyte concentration in biological, foodstuff, and environmental samples, there is observed a decrease in method performance using classical methods for the data processing of MS measurands. How do we address this problem? It has been considered via innovative stochastic dynamic Equations (1) and (2), capable of exact quantifying analytes [55,56,60–67]. Formula (2) is derived from Equation (1), where 'I' denotes the intensity of the MS peak. There are excluded imaging methods for quantifying analytes or approaches capable of spatially resolving the chemical composition of a surface sample [68].

Formula (2) overcomes a set of difficult classical quantitative MS concepts [55,56,60–67]. Superior chemometrics is explained with the help of Formula (2) to quantify exactly the fluctuations in measurands in a short period of scan time. It is capable of determining the 3D molecular and electronic structures of chemicals mass-spectrometrically, when it is used complementarily with Arrhenius's Equation (3). The functionality $D''_{SD} = f(D_{QC})$ has shown |r| = 0.9999_4 [65].

To summarize, the study deals with the quantitative and 3D structural stochastic dynamic MS biomonitoring of mixtures of antibiotics PARA, ATE, and PRO in the presence of benzalkonium chloride surfactants BAC-C12, BAC-C14, BAC-C16, and BAC-C18 in biota using mussel tissue, sludge cakes, and a treated effluent.

$$D_{SD}^{tot} = \sum_{i}^{n} D_{SD}^{i} = \sum_{i}^{n} 1.3194.10^{-17} \times A^i \times \frac{\overline{I_i^2} - \left(\overline{I_i}\right)^2}{\left(I_i - \overline{I_i}\right)^2} \tag{1}$$

$$D_{SD}^{'',tot} = \sum_i^n D_{SD}^{'',i} = \sum_i^n 2.6388.10^{-17} \times \overline{I_i^2} - \left(\overline{I_i}\right)^2 \tag{2}$$

$$D_{QC} = \frac{\prod\limits_{i=1}^{3N} v_i^0}{\prod\limits_{i=1}^{3N-1} v_i^s} \times e^{-\frac{\Delta H^{\#}}{R \times T}} \tag{3}$$

2. Results and Discussion

2.1. Mass Spectrometric Data

2.1.1. Mass Spectrometric Fragmentation Reactions of Paracetamol and Its d$_3$-Derivative

Paracetamol shows fragmentation path CID (m/z 152)→152, (134,) 110 (Figures 2, S1, S3 and S4) [69–79] (see chemical diagrams of species in Figure S2). Its dimer [2M+H]$^+$ shows fragmentation path CID (m/z 303)→303, 152 [69,75]. The ammonium adduct [2M+NH$_4$]$^+$ exhibits a low-abundance peak at m/z 320 [75]. MS analysis of PARA radical-cations has been reported [72]. Fragmentation processes, involving a radical-cation mechanism of bond cleavage, have been proposed [77]. PARA tends to stabilize not only the Cu^{2+} adduct, but also adducts of alkali metal ions and NH$_4^+$ cation. There are species of type [M+NH$_4$]$^+$ (m/z 169), [M+Na]$^+$ (m/z 174), [M+K]$^+$ (m/z 190), [2M+NH$_4$]$^+$ (m/z 320), [2M+Na]$^+$ (m/z 325), and [2M+K]$^+$ (m/z 341), respectively [79]. As Figures S5–S8 reveal, the abundance of peaks depends on the applied voltage, presence of formic acid, and analyte concentration. The same is true for the peak of protonated analyte [M+H]$^+$ and its major fragmentation product of N–C bond cleavage, [M-CH$_3$CHC=O]$^+$, at m/z 152 and 110. The data on d$_3$-PARA show similar fragmentation patterns together with some adducts. The peak at m/z 331 belongs to [2.d$_3$-M+Na]$^+$. There is an observed fragmentation reaction CID (m/z 152)→152, 110, 93 [78]. MS spectra of PARA in a sludge cake and biota (Figures 3, S9, S10 and S13) show competitive fragmentation mechanisms causing not only charged cations, but also cation radicals.
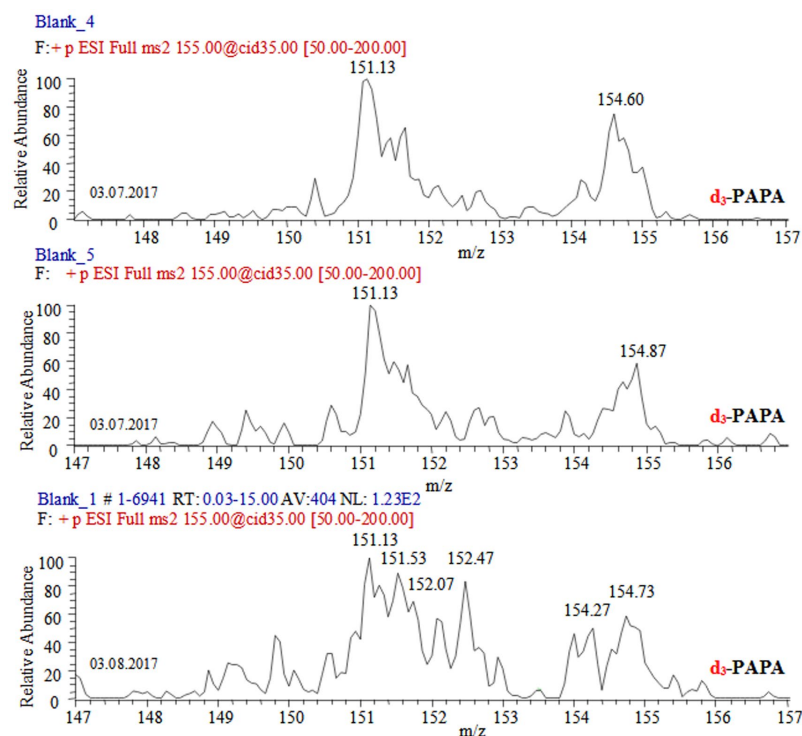
Figure 2. CID-MS/MS spectra of molecular cation [M+H]$^+$ of d$_3$-deuterated paracetamol at m/z 155 assessing within-day and between-day variability of mass spectrometric measurands.
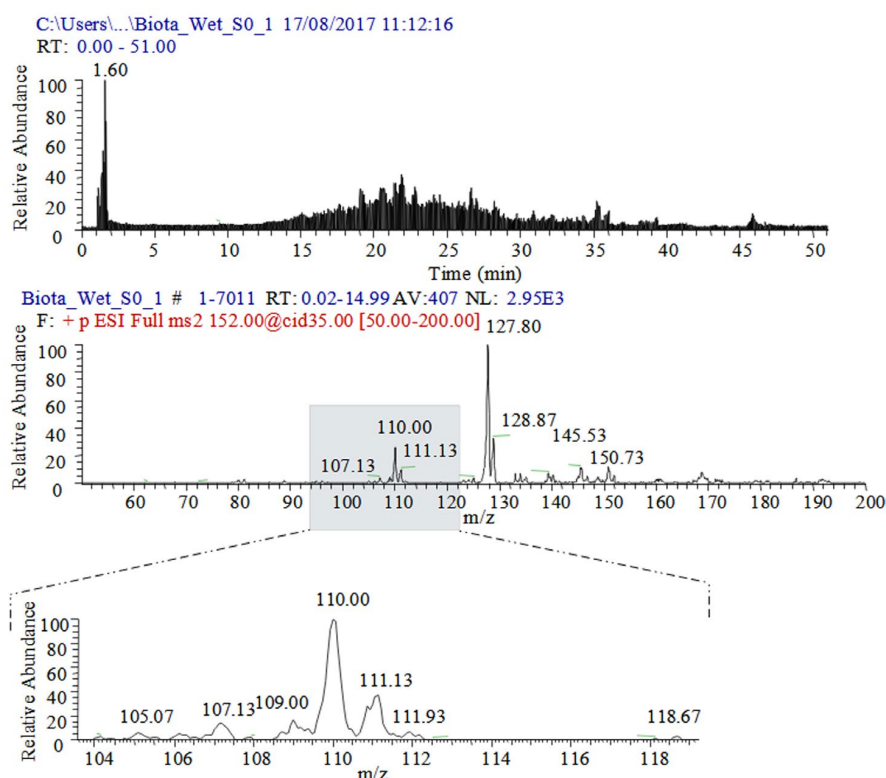
Figure 3. The total ion current (**top**) of standard sample of wet biota; CID-MS/MS spectrum of molecular cation [M+H]$^+$ at m/z 152 of paracetamol (**bottom**).

2.1.2. Mass Spectrometric Fragmentation Reactions of Biocides

Surfactants BAC-C12, BAC-C14, BAC-C16, and BAC-C18 exhibit molecular cation [M]$^+$. The major fragmentation path shows the loss of 92 Da of toluene (Figure S11). Regarding the MS spectra of PARA and its d$_3$-PARA derivative (Figure S12), depending on the experimental conditions, there are competitive fragmentation reactions causing more than one conformational and tautomeric form of product ions (Figures S9 and S10). Although the major fragmentation MS path of these surfactants is associated with the loss of the hydrophilic head of the compounds, the product ion consisting of a charged hydrophobic tail exhibits a complex conformational preference and electronic effects (Figures S13 and S14). Therefore, after examining only experimental measurands in CID-MS/MS and SRM operation modes, a lack of assignment of observable peaks to ions remains. Consider the shape of the SRM spectrum of BAC-C12 (Figure S11) and the proposed chemical 2D diagrams and electronic structures of ions at m/z 212 and 213.

2.1.3. Mass Spectrometric Fragmentation Reactions of β-Blockers

Propranolol shows the [M+H]$^+$ cation at m/z 260 [80]. The fragmentation paths depend on CE, pH, etc. [1,80–95]. With increasing CE, there is a low-abundance ion at m/z 183, due to the cleavage of the [C$_3$H$_9$N]^0 fragment and solvent water [1,80,83] (Figures S2 and S15). The peak at m/z 282 of the MS spectrum of PRO at CE = 30V is assigned to the [M+Na]$^+$ adduct. The same is true for ATE MS reactions (Figure S16). Their identical structural (2,3-dihydroxy-propyl)-isopropyl-ammonium fragment causes peaks at m/z 145, 105, 101, 83, and 64, respectively. ATE exhibits the [M+H]$^+$ cation at m/z 267. Quantitative analysis was carried out, examining the [M+H]$^+$ cation at m/z 260 and 267 of PRO and ATE in the mixture. Employment of the SRM and SIM modes leads to pairs of MS peaks at 260/261 and 267/268 (Figure S17). Classical quantitative methods look at average m/z data on MS peaks at m/z 260.5 (SRM) and 262.07 (SIM) (PRO), as well as 267.52 (SRM) and 267.82 (SIM) (ATE). The matrix affects significantly not only the m/z data compared with the results from the fragmentation paths of standard samples, but also product ions [86–95] (Figure S18).

Owing to the fact that there is used only an MS peak of the [M+H]$^+$ cation in both the cases, excluding a statistically representative set of fragmentation species, there is particular importance in accounting for the molecular conformations and electronic effects of protonated antibiotics in order to assign statistically different sets of m/z data on two SRM and SIM spectra of standard samples of antibiotics and their mixtures in environmental and biological matrixes. For the purposes of 3D structural analysis and empirical demonstration of the assignment of the [M+H]$^+$ cation at m/z 260 of PRO in the complex sample matrix, there is used a statistically representative set of MS peaks at m/z 260, 283, 157, 116, and 98 found in the MS spectrum in soil [80]. The same fragmentation species have been found in the MS spectrum of PRO in biological samples [81,91]. Owing to the proposed two competitive mechanisms of formation of the MS ion at m/z 183, our study examines the correlation between MS data and theoretical quantum chemical ones looking at ions 183$_a$ [80,81,90] and 183$_b$ [82]. The MS ion at m/z 116 in the CID-MS/MS spectrum of PRO has been observed examining tandem MS/MS processes of ATE and studying the ions' CID interaction of the [M+H]$^+$ cation at m/z 267 [84]. The peak at m/z 116 has been used to determine PRO in the liver, brain, and kidney thin tissue, as well [85,94]. In addition to the peak at m/z 116, ATE exhibits a set of ions depending on the experimental conditions [96–100]. These are peaks at m/z 225, 208, 190, 173, 162, and 145 [84,96–100]. Moreover, there are peaks at m/z 133, 115, and 107 [94] (Figure S19).

2.2. Determination of Stochastic Dynamic Diffusion Parameters

The capability of Equation (1) in determining the 3D molecular structures of analytes, when it is used complementarily with Equation (3), has already been reviewed [60]. In this light, herein, we prove its validity and compatibility with Equation (2). In verifying empirically the validity of Equation (1), we can explore the results from SRM data on the MS ion at m/z 110 of PARA of its MS/MS spectra of the [M+H]$^+$ cation at m/z 152 (Table S2). The new data on variables of PARA show lnP1 = 17.0532. Therefore, Equation (1) shows that the MS law is valid for the temporal distribution of measurands of PARA, as well. Details of the statistical parameters A^i are presented in Figure S20. Calculation tasks have been discussed previously [55,56,60–67]. The latter figure illustrates the relation between the D'_{SD} and D''_{SD} parameters, showing $|r| = 0.9995_3$. The deviation from $|r| = 1$ is a result of the error contribution of the data processing of the temporal distribution of intensity with respect to the scan time or function $(I–<I>)^2 = f(t)$ fitted to the SineSqr function, thus producing statistical parameter A^i (Figure S20).

2.3. Quantitative Data on Biocides

We shall support our method by highlighting how the D''_{SD} parameters are determined per span of scan time. We shall justify the view that exact relations are obtained when there are quantified fluctuations of measurands with a short span of scan time. The question that we need to address is "Which criteria determine a set of MS measurands with respect to a concrete span of scan time as the true one?", or which methods are used in order to validate the parameters of Equation (2). In doing so, we use data on the selected reaction monitoring mode of the PARA [M+H]$^+$ ion at m/z 152 of segments of the MS method, where segment (i) has collected a full mass scan set of variables. There are examined segment raw data QC_High_SRM_SEG_CE40_i.raw (i = 1–3) [101,102] (Figure S12). Table S2 lists the output, only, of the fragmentation ion at m/z 110 for the SRM operation mode, while Tables S3–S6 list results from the CID-MS/MS spectra of PARA of its [M+H]$^+$ cation at m/z 152 depending on experimental conditions such as CE and the presence of formic acid. Chemometrics of the normality Shapiro–Wilk test together with ANOVA data in Tables S2–S6 are summarized in Tables S7 and S8. Data on quality control standard samples of a mixture of antibiotics QC_H_SRM_CE40_3 (segment 3, Table S2) reveal three groups of m/z parameters that are mutually significantly different from the perspective of chemometrics (Table S8). These are a subset of variables of segment 3, shown as QC_High_SRM_SEG_CE40_3_1, QC_High_SRM_SEG_CE40_3_2, and QC_High_SRM_SEG_CE40_3_3. The same is true for the

recorded two sets of m/z variables of the same ion of segment (2) (QC_High_SRM_SEG_CE40_2_1 and QC_High_SRM_SEG_CE40_2_2). The chemometric analysis of datasets of measurands at m/z 110.1, i.e., QC_High_SRM_SEG_CE40_3_3, QC_High_SRM_SEG_CE40_2_1, and QC_High_SRM_SEG_CE40_1, is statistically equal. In other words, correlative analysis and determination of the D''_{SD} parameters of Equation (2) within the framework of three segments of MS spectra is carried out using those sets of measurands that are statistically significantly equal, or those with values at m/z 110.065. Therefore, there are distinguished quantitatively three sets of peaks at m/z 110: $110.84_{49} \pm 0.05985$, $110.06_{525} \pm 0.04709$, and 110.23885 ± 0.04898. The number of the subset of variables is not extensive when looking at whole datasets of average values over the whole period of measurement. Results from sector (3) (QC_High_SRM_SEG_CE40_3) show a value at m/z 110.0673. In other words, our approach does not ignore measurable sets of low-abundance variables and their fluctuations.

The examples could be multiplied, in fact, without limit when looking at the dataset of measurands in environmental and biological samples of antibiotics and biocides. The results provide compelling evidence for the advantages of our method. The analysis of the effluent, treated sludge cake, and biota show that PARA and its d$_3$-derivative in the presence of antibiotics or biocides reveal peaks at a range of m/z 107–115, which further complicate not only the qualitative assignment of products, but also the quantification of those single analytes in mixtures, as well as the deuterium exchange processes of d$_3$-PARA, if any.

Quantitative data on biocides in biota show $r^2 = 0.9309$–0.985 (Figures S9, S11 and S21) using the classical approach to quantify the average total intensity of MS peaks over the whole period of measurements [1,103]. The results were data-processed via the ICIS algorithm of peak detection. The Savitzky–Golay smoothing function with baseline correction was used. The ICIS algorithm involves a trapezoidal integration approach [1,5–7,104]. In order to account for the effect of the smoothing function on chemometrics, herein, we examined the same relationships, but applying baseline correction and TIA (Figures 4 and S22–S24). Figure S25 illustrates relationships among the concentrations of BAC-C12 and BAC-C14 in biota showing $|r| = 0.9874_5$ and 0.9922_3. Despite this, the ICSI or TIA methods show low $|r|$ parameters and high sd(yEr$\pm$) for mean values. The linear equation obtained via the direct application of TIA of BAC-C14 is $y = -16.1_{3779} \pm 14.6_{133} + 6.5_{4102} \pm 0.3_{3481}.x$. The error contribution of the data-processing algorithm affects the main value of the intercept and slope of linear regression, respectively, and the correlation equations. The reliability of quantitative data is complicated when examining biota. There are competitive fragmentation reactions producing both mono-cations and cation radicals. The CID-MS spectra of PARA of freeze-dried biota show peaks at m/z 108.07 and 109.07. The wet sample shows MS ions at m/z 107.07, 110.07, and 111.1 (Figures 1, 3, 4 and S26). The mixtures of biocides show pairs of ions at m/z 211 and 212 (BAC-C12) and 239 and 240 (BAC-C14), instead of a single ion according to the common fragmentation scheme. The data processing of isotopologies in biota via the latter algorithms yields high sd(yEr$\pm$) values (Figures S27 and S28). Either by the ICIS or TIA algorithm, with or without baseline correction, the uncertainty of the analytical results is increased.

The task can be completed precisely by Equation (2). ICIS and TIA are incapable of providing reliable analytical data on environmental and biological samples, particularly when there are tautomers and fragmentation reactions involving different molecular-level mechanisms, leading not only to cations, but also to cation radicals. Moreover, it is true that ca. 25% of pharmaceutics exist in more than one tautomeric form, in addition to the fact that almost all antibiotics are characterized by multiple ionizable protonation positions in their molecules [105]. Reference [63] concerns the same problem of quantifying LMW antibiotics in biological fluid.
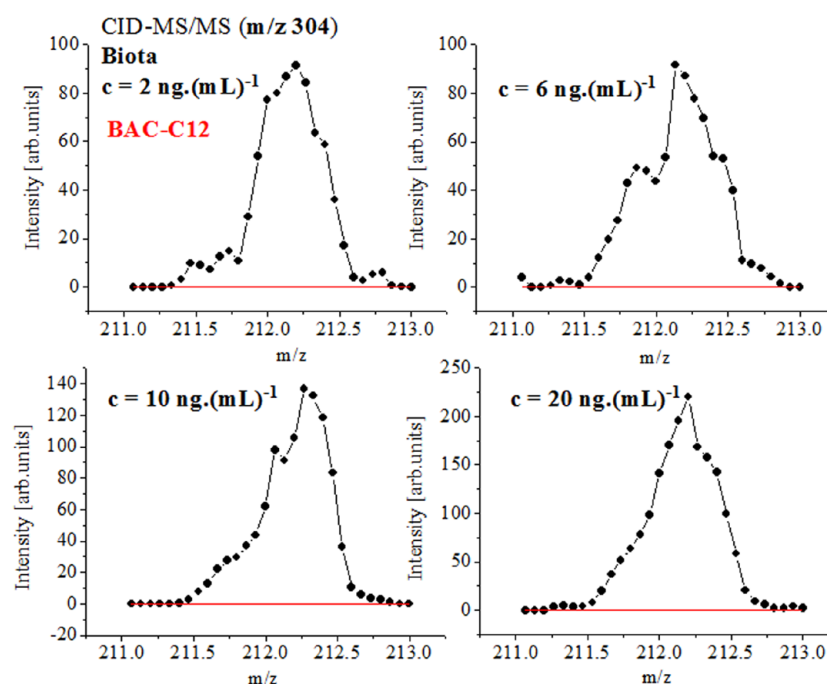
Figure 4. SRM spectra of analyte BAC-C12 in biota, using analyte molecular cation [M]$^{+}$ at m/z 304 at concentrations c = 2, 6, 10, and 20 ng.(mL)$^{-1}$; baseline correction of isotopologies; data on trapezoidal integration approach (see also Figures S22–S24).

Thus, the following paragraph focuses on the quantitative analysis of biocides using Equation (2). We shall describe the advantages of Formula (2) compared with the results from the ICIS or TIA methods presented so far.

Table S9 summarizes m/z data on BAC-C12 and BAC-C14 in biota at concentrations c = 2–80 ng.mL^{-1}. ANOVA and t-tests show (Tables S8 and S10) two sets of m/z values at $212.2_{2211} \pm 0.12988$ and m/z 211.6 at c = 2 ng.mL^{-1} (BAC-C12), which are statistically significantly different. At c = 6 ng.mL^{-1} are distinguished three sets of measurands at m/z 213, 212, and 211.5 (Table S8, Figure S10). There are three elemental compositions, molecular conformations, and electronic structures of BAC-C12 species ($212.2_{1401} \pm 0.1001$, $212.5_{4356} \pm 0.12232$, and $211.7_{86} \pm 0.15203$.) Datasets at m/z $212.22_{211} \pm 0.12988$ and $212.2_{1401} \pm 0.1001$ of BAC-C12 ions at c = 2 and 6 ng.mL^{-1} are statistically not significantly different. The ion at m/z 212.2 belongs to one and the same ion at two concentrations.

Further, we shall come to see that Equation (2) accounts precisely for the fluctuations in the m/z and intensity data on MS peaks, thus producing excellent-to-exact quantification and 3D structural analysis, despite the complexity of the isotope shape. Figures 5, 6 and S32 show that the quantification of biocide BAC-C12 in biota employing the D''_{SD} parameter and assessing the relationship $\ln[D''_{SD}]$ = f(conc.) yields $|r|$ = 0.9999_1–0.9905_8, examining c = 2–80 ng.(mL)$^{-1}$. Conversely, the ICIS and TIA algorithms produce $|r|$ = 0.98924 (Figure S21). There has been obtained $|r|$ = 0.999 when studying the same set of analytes in sludge [5]. Data on PARA and d$_3$-PARA c = 5–400 ng.(mL)$^{-1}$ show r^2 = 0.997. Quantification of BAC-C12 and BAC-C14 yields r^2 = 0.987 and 0.983 [1,6,7]. The analysis of the peak at m/z 211.75 $\pm$ 0.15 of BAC-C12 ions in biota using the [M+H]$^{+}$ cation at m/z 304 (Tables S11 and S12 and Figure 6) produces $|r|$ = 0.9972_1 and 0.9841_1 when employing the equation D''_{SD} = f(conc.) Again, there is improved method performance. The analysis of BAC-C14 yields $|r|$ = 0.9918_8 within concentration range c = 20–80 ng.(mL)$^{-1}$.
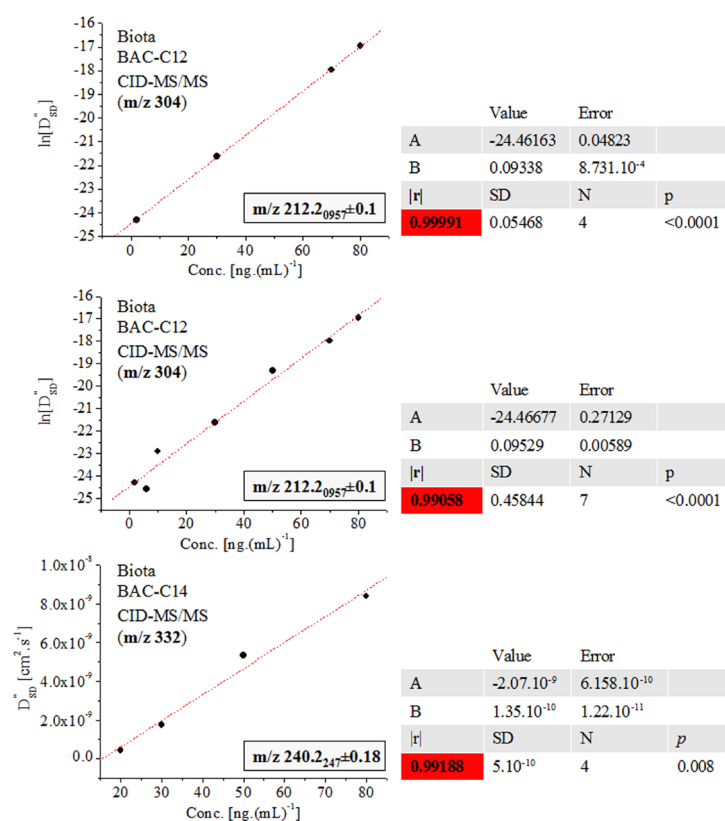
Figure 5. Linear functional relations $\ln[D''_{SD}]$ = f(conc.) and D''_{SD} = f(conc.) of fragmentation ions at m/z 212.2$_{096}$ and 240.2$_{247}$ of SRM spectra of molecular cation $[M]^+$ at m/z 304 and 332 of surfactants BAC-C12 and BAC-C14 in biota; chemometrics; the coefficient of correlation is highlighted in red.
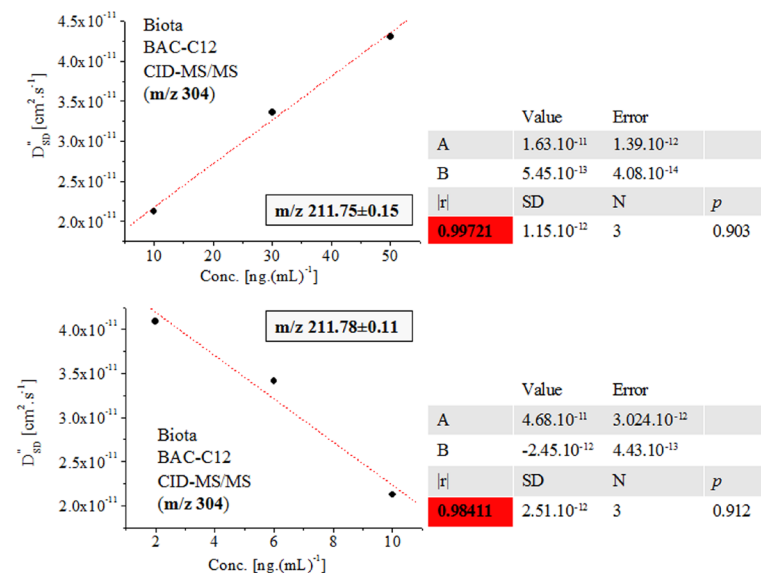
Figure 6. Linear functional relation D''_{SD} = f(conc.) of fragmentation ions at m/z 211.75 and 211.78 of SRM spectra of molecular cation $[M]^+$ at m/z 304 of surfactant BAC-C12 in biota; chemometrics.

2.4. Quantitative Functions between Mass Spectrometric Stochastic Dynamic Diffusion Parameters and Theoretical Total Intensity Variables with Respect to Experimental Parameter Collision Energy

Since the main goal of the current paper is to advocate for a general innovative approach to quantifying analytes in complex environmental and biological matrixes, mass-

spectrometrically via Equation (2), in this short subsection, we shall direct the reader's attention to Equation (4), appearing valid for MS data on labetalol [64].

$$\overline{I^{TOT,q}} = \frac{1}{2} \times \frac{A_I^q}{A_D^q} \times D_{SD}^{'',tot} \tag{4}$$

Equation (4) is derived from Equation (1) (see Equation (A6) in [64]). It connects the theoretical average intensity data on analyte MS ions obtained toward CE and the D''_{SD} of Equation (2). Statistical parameters A_D^q and A_I^q are functional amplitudes of the SineSqr function fitted with relation $D''_{SD}{}^q$ = f(CE) and $<I>^q$ = f(CE) of qth MS fragment ion. We look at new empirical proof of the validity of Equation (4). It has been found by examining PARA measurands (Table S5). Figures S29 and S30 depict the relations of $D''_{SD}{}^q$ = f(CE) and $<I>^q$ = f(CE) of MS ions of PARA at *m/z* 60 and 64. The theoretical $<I>_{theor}$ data on ions with respect to CEs and A_D^q, A_I^q parameters (Table S12) correlate with the experimental $<I>_{exp}$ ones and show $|r| = 0.9942_9$ and 0.96501. Since, so far, we have considered only two cases of the application of Equation (4) for the latter purposes, we are unable, currently, to assess the apparent violation of its validity.

2.5. Theoretical Data

2.5.1. 3D Molecular Conformations and Electronic Structures of Analytes and Energetics

The calculation of the D_{QC} parameters of Equation (3) has been discussed [61,63,65,66]. However, we need to discuss the correlation between the 3D molecular conformation of MS ions and their energetics, thus highlighting the advantages of Equation (3), consisting of significant sensitivity and selectivity and capable of distinguishing quantitatively among molecular structures, exhibiting subtle electronic effects (Table S15). Figures S31–S33 detail the static and MD DFT results from ions in GS and TS states. Table S16 summarizes the atomic coordinates of fragmentation ions, allowing us to extract geometry parameters such as bond lengths and angles. The energy difference in the fragmentation species of surfactants such as ions 212_a and 212_b is $\Delta E^{TOT} = |0.015|$ a.u. The difference in the energetics of molecular ion $[M+H]^+$ of PARA and d_3-PARA is of the same magnitude order ($\Delta E^{TOT} = |0.01|$ a.u.). In these and many more cases of ions [60,61,63,65,66], there is provided ample proof favoring Equation (3) as a sensitive and selective tool, allowing us to distinguish among molecular species exhibiting comparable energetics. There are almost identical ΔE^{TOT} ions of tautomers of PARA and d_3-PARA (Figure S15). The examples of species provide us with real insights into the complexity of the electronic effects and dynamics of MS ions, which are unable to be tackled precisely when examining only free Gibbs energy data on the global minimum of PES (Table S17). Despite the fact that there is $\Delta E^{TOT} = |0.01|$ a.u. of ions 152_a and 155_a for the molecular cation of PARA and d_3-PARA, the difference in the D_{QC} parameter is $\Delta D_{QC} = |3.371|$ (Table 1).

2.5.2. Determination of Quantum Chemical Diffusion Data

Details on the calculation tasks of the D_{QC} parameters of Equation (3) can be found in [62]. Methodologically, we use vibrational data on MS ions at GSs and TSs. Variations and changes in the energetics of species can be examined adequately via Born–Oppenheimer MD. Table 1 summarizes the D_{QC} parameters of the studied herein MS ions.

2.6. Correlative Data on Mass Spectrometry and Quantum Chemistry

We return to the major question that we posed at the beginning of the study: How does Equation (2) serve as a tool to determine the 3D molecular and electronic structures of analytes mass-spectrometrically, even examining multicomponent environmental and biological samples, having complex sample matrix effects? In the latter response, we shall focus on the chemometrics of relation D''_{SD} = f(D_{QC}). In line with our previous studies devoted to the same issue [61,63,65,66], achieving such a goal requires the assessment of the statistical significance of the mutual relationship between D_{QC} and D''_{SD} data on ions

belonging to one and the same molecular structure. Figure 7 shows the chemometric results from PARA at m/z 152, 158, 174, 301, and 325 depending on CE (Tables 1 and S5). There are $|r| = 0.9979_8$ at CE = 10 V and $|r| = 1$–0.9936_1 at CE = 25 V.

Table 1. Theoretical D_{QC} parameters of Equation (3) according to most stable analyte 3D molecular and electronic structures of species at ground and transition states and energetics (Table S15); frequencies and atomic coordinates are listed in Tables S16 and S17.

m/z	Form	D_{QC}	m/z	Form	D_{QC}
110	110	2689.768			
152	152_a	101.531209	155	155_a	98.1605
	152_b	646,318		155_b	3.45123
158	158	367.4416	161	161	2902.9217
174	174	3009.373	177	177	42,352.98
325	325	21.08666	301	301	14.141939

Further, little contract might be observed in Figures S34 and S35, depicting data on d_3-PARA and propranolol (Table 1, Tables S5–S14). In the former case, there is obtained $|r| = 0.9993_1$. Relation $D''_{SD} = f(D_{QC})$ of PRO ions at m/z 260, 157, and 116 shows $|r| = 0.9916_1$.
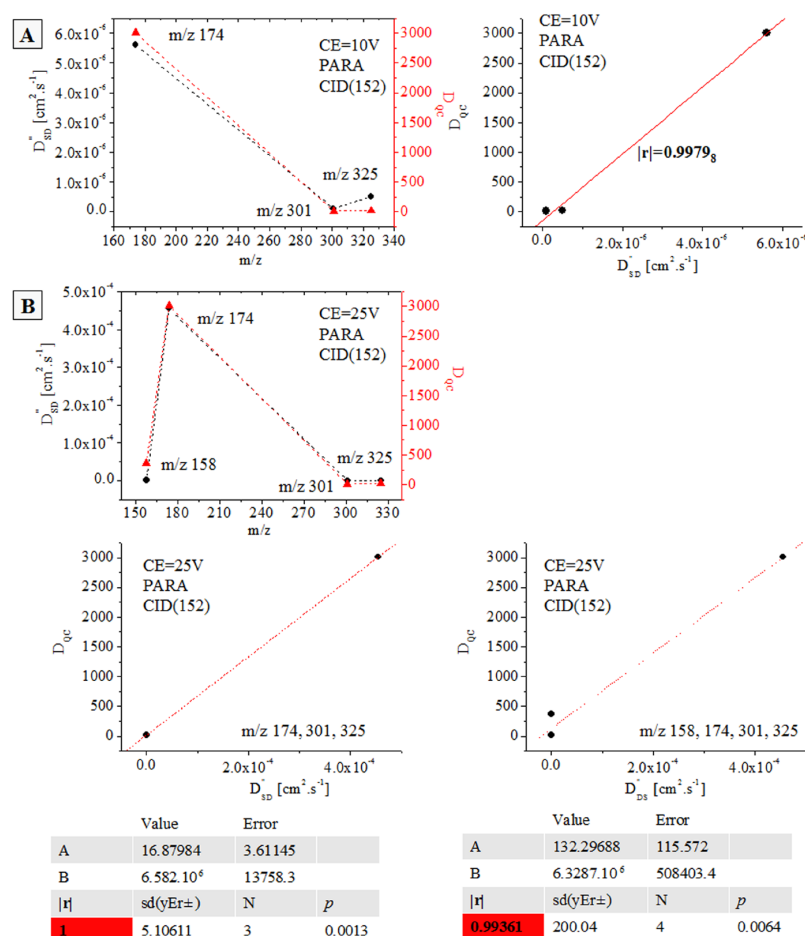
Figure 7. Functional relationships between D''_{SD} [cm^2.s^{-1}] and D_{QC} data on Equations (2) and (3) of fragmentation ions of CID-MS/MS reactions of molecular ion [M+H]$^+$ of paracetamol at CE 10 (**A**) and 25 (**B**) V; chemometrics.

3. Discussion

Since the purpose of the study is to gain insights into quantitative functionalities among MS measurands of analytes' molecular and fragmentation peaks, the physico-chemical properties and parameters of molecular and ionic species, and their 3D molecular and electronic structures, as well as experimental factors and parameters of measurements, this section might be regarded as room for debate, for which we suggest that the discussion helps the reader to understand whether Equations (1) and (2) are capable of providing not only the exact quantification of analytes in complex biological and environmental matrixes, but also the simultaneous 3D structural determination of the same compounds and samples. However, before embarking on a discussion of the advantages of Equations (1) and (2), we provide a few remarks on the data reported so far.

To begin with, methodological contributions devoted to developing quantitative methods for the analysis of datasets of measurands and those devoted to elaborating methods for 3D structural MS analysis are not equally frequent. Therefore, developed methods for simultaneous quantitative and 3D structural analyses, and approaches capable of providing the exact determination of the amounts and structural parameters of molecules, are restricted. We draw the reader's attention to the fact that Equation (2) is one of the scarce examples of formulas used for both quantitative and 3D structural analyses. However, the latter statements lead us to a logical question: Why should we be forced to become aware of details of analytes' 3D molecular structures, owing to the fact that quantitative analytical mass spectrometry represents different areas of structural mass spectrometry? Routinely, we process MS-based quantification as a separate research task. It is well known that with such distinctions in research tasks, we are completely able to characterize and quantify analytes mass-spectrometrically. This combined set of research tasks would seem to complicate the further experimental design of the MS analysis of environmental and biological samples. An answer to such a question, if any, would be that, since stochastic dynamic model Equation (2) is a novel analytical MS law, it would be best to provide, herein, an immediate illustration of the crucial importance of the capability of Formula (2) in quantifying and determining the 3D structures of analytes via MS for the purpose of the quantitative analysis of complex environmental and biological samples. Our earlier and most recent outcome of the application of Equation (2) to determine exactly LMW analytes in biological fluids [63]—which, however, largely matches the results from the current study—perhaps best illustrates the advantages of our stochastic dynamic theorization of MS phenomena via Equation (2) over classical quantitative approaches. For instance, these include the ICIS or TIA algorithms, dealing with the integration of the area of the MS shape of analyte fragment peaks as a continuous function of the m/z values with respect to MS intensity, instead of as discrete random variables and their fluctuations with a short span of scan time, as according to Formulas (1) and (2). As the MS analysis of metronidazole in clinical human urine has demonstrated [63], analyte molecular ion $[M+H]^+$ is characterized by a set of statistically significantly different m/z variables depending on the experimental conditions, but explicitly highlighting low analyte concentrations at a range of 2.5 to 25,000 ng.(mL)$^{-1}$. It has been found that there are observed mass-spectrometrically two datasets of measurands at m/z 172.071_8 and 172.040_{81} of the $[M+H]^+$ cation. As can be expected, the employment of classical quantitative approaches to determine the analyte concentration yields $|r| = 0.9939_5$–0.9940_4 using linear calibration equation $I^{TOT} = f(conc.)$, where I^{TOT} is determined via the ICIS or TIA algorithms. The decrease in method performance has been explained with the fact that, on the one hand, there are quantified isotope shapes of two different m/z quantities, which even can belong to two different analytes in complex biological samples, when there are determined unknown compounds. On the other hand, the error contribution to the mathematical data processing of MS patterns by means of the ICIS or TIA algorithms is significant, due to the large sd(yEr±) values of integration approaches. Due to these reasons, we suggest that the reliable and exact quantitative analysis of such complicated cases of fluctuations of MS measurands at very low analyte concentrations and complex matrix effects can be carried out exactly,

accurately, precisely, selectively, and sensitively only via Equation (2) and the simultaneous quantitative and 3D structural analysis of analytes with respect to the experimental conditions of measurements. These combined research tasks allow us to assign exactly statistically different sets of measurable variables to corresponding molecular conformations and electronic structures of analytes. It has been found that the aforementioned MS peaks of metronidazole at m/z 172.071_8 and 172.040_{81} belong to its two different tautomeric forms. The performed quantitative analysis based on two different calibration statistical equations $D''_{SD} = f(\text{conc.})$ of two fragmentation peaks has resulted in $|r| = 1$. Turning to the results from this study in quantifying biocides BAC-C12 and BAC-C14 in biota, it can be easily shown an analogous cases of the temporal distribution and variations of MS measurands of these analytes in complex matrix samples depending on the experimental conditions, particularly highlighting a low analyte concentration as a major factor causing the observation of sets of statistically different m/z measurable variables belonging to different molecular conformations and electronic structures of analyte fragmentation species. Due to these reasons, the employment of the ICIS or TIA algorithms, quantifying the isotope shape area of function $m/z = f(I)$, yields $|r| = 0.9304$–0.9856. Conversely, as the results from our analysis using Equation (2) show, there are statistically significant sets of variables of fragmentation ions at m/z 212 of CAB-C12 obtained as a result of the SRM tandem fragmentation mode of the molecular cation of analyte $[M+H]^+$ at m/z 304 (Tables S8 and S9). The statistical linear calibration models $\ln D''_{SD} = f(\text{conc.})$ and $D''_{SD} = f(\text{conc.})$ have resulted in exact method performance, showing $|r| = 0.9999_1$–0.9905_9 and 0.9972_1. There are examined MS peaks of BAC-C12 at m/z 212.209 ± 0.1 and 211.75 ± 0.15. Thus, again, there is observed a highly reliable and very prominent quantitative analysis when we use Equation (2) instead of classical quantitative MS approaches based on the aforementioned algorithms. The new data presented in this paper on the MS quantitative analysis of mixtures of biocides and antibiotics in biota and sewage sludge show clearly the capability of the exact and reliable processing of complex isotope shapes of MS measurands, obtained as a result of competitive processes of tautomers and mechanisms involving the formation of cations and cation radicals, which is not only not universal, but also is beyond the capability of classical quantitative methods for the data processing of MS measurands. It is reasonable to assume, therefore, that classical automated algorithms of data processing of observable variables of such complex MS patterns are of little use when dealing quantitatively with the analysis of environmental and biological multicomponent samples of unknown analytes, very low analyte concentrations, and sample matrix effects. Furthermore, owing to the fact that the determination of analytes within the framework of the stochastic dynamic theory and model Equation (2) is carried out without the presence of IS, it is obvious that the innovative method allows researchers to determine quantitatively and structurally by mass spectrometry any unknown analyte in a complex mixture whose measurable parameters do not fit exactly with the available ISs or there is a lack of suitable internal standards. The latter remark is associated with the fact that both quantitative and 2D structural analytical methods for mass spectrometry, so far, use mainly ISs. Thus, under the so-called confirmed structure, there is understood currently (a) a reported exact mass; (b) an unequivocally determined molecular formula, and (c) a single confirmed structure, which is obtained by means of IS. However, often, environmental and biological samples contain analytes lacking suitable ISs. Therefore, even 2D structural MS analysis produces a so-called possible structure or tentative candidates of a 2D chemical diagram. On the other hand, we should distinguish between so-called 2D chemical diagrams and 3D molecular structures as well. The 2D diagrams are obtained according to the rule of the degree of unsaturation, in addition to concepts of atomic valence and oxidation states. We note the following statements: (a) " . . . the sum of the valences of all the bonds formed by an ion is equal to the valence of the ion", and (b) " . . . the stoichiometry must be obeyed by electro neutrality principle" [106]. However, 2D structures or 2D diagrams do not tell us anything about the chemical reactivity and the chemistry of the molecules. Why? The term "molecular structure" means a generic property determined by an ensemble of atoms in a

molecule [106]. However, analytical statements, claiming 3D molecular structures, should be based on electronic structural analysis, which is reliable only when there is information about the electron density maps of the ensemble of atoms in the molecules. The electron density maps are proof of the probability density distribution, which is observable experimentally. These maps determine the probability of determining electrons at infinitely small volumes and positions in the 3D space [107]. The so-called total energy is determined on the basis of the electron density maps. Therefore, any 3D molecular model or 3D molecular structure is characterized by a unique to total energy quantity. In other words, from the perspective of structural chemistry, under a 3D molecular structure, there is understood a 3D molecular conformation and corresponding electronic structures, which are unique as a whole. There is a lack of corresponding disordered structural fragments.

Of course, an objection to the latter statements could be made by arguing that this study deals with the complicated case of the molecular structures of biocides showing a set of 3D molecular conformations, thus leading to a significant variation in m/z measurands and corresponding fluctuations in the observable m/z and intensity parameters of fragmentation ions. However, a part of the answer to such a question, if any, lies in the fact that the statements outlined above are obvious looking at the results from work [63] and those reported herein of the analysis of biocides in biota and sewage sludge.

Perhaps the most astonishing empirical evidence for the latter statements has been provided looking at the results from this study, analyzing the temporal distribution of measurable variables of standard PARA and its d_3-derivative, particularly examining the fragmentation reactions of MS molecular ions $[M+H]^+$ and $[d_3\text{-}M+H]^+$ at m/z 152, 155, 158, 174, 301, and 325, yielding the exact coefficient of linear correlation between D_{QC} and D''_{SD} data on CE = 25 V (Figure 7).

4. Materials and Methods

4.1. Chemicals and analytical instrumentation

Paracetamol (acetaminophen, 4′-hydroxyacetanilide, N-(4-hydroxy-phenyl)-acetamide), atenolol (2-[4-(2-hydroxy-3-isopropylamino-propoxy)-phenyl]-acetamide), propranolol (1-isopropylamino-3-(naphthalen-1-yloxy)-propan-2-ol), benzyl-dodecyl-dimethyl-ammonium chloride (BAC-C12), benzyl-dimethyl-tetradecyl-ammonium chloride (BAC-C14), benzyl-hexadecyl-dimethyl-ammonium chloride (BAC-C16), and benzyl-dimethyl-octadecyl-ammonium chloride (BAC-C18) were Sigma Aldrich products.

Thermo Finnigan LC (Massachusetts, USA) instrumentation equipped with a Micro AS autosampler and MSPump Plus was used. LC columns, namely the Waters Xbridge C18 column (Milford, USA; 1.0 × 100 mm ID, 3.5 μm), Waters Xselect charged surface hybrid C18 column (2.1 × 150 mm ID, 3.5 μm), Waters Xselect high-strength silica T3 column (1.0 × 100 mm ID, 3.5 μm), and a Phenomenex KrudKatcher Ultra 0.5 micron in-line filter, were used [1]. Experimental conditions of MS measurements are listed in Table S1.

The study used the MS database on MS measurements available in [101,102].

4.2. Sample Preparation Methods, Samples, and Solutions

See details in [1,5–7,101,102,108].

4.3. Theory/Computations

The GAUSSIAN 98, 09; Dalton2011, and Gamess-US [109–111] program packages were employed. Ab initio and DFT molecular optimization was carried out by means of B3LYP, B3PW91, and ωB97X-D methods. Truhlar's functional M06-2X was used [112]. The algorithm by Bernys was used to determine GSs. The stationary points at PES were obtained by harmonic vibrational analysis. The basis set cc-pVDZ by Dunning and 6-31++G(2d,2p) and quasirelativistic effective core pseudo-potentials from Stuttgart–Dresden(–Bonn) were used. MD computations were performed by ab initio BOMD, which was carried out with the M062X functional and SDD or cc-pvDZ basis sets, as well as without considering the periodic boundary condition. Allinger's MM2 force field was utilized [113,114]. The low-

order torsion terms were accounted for with higher priority than van der Waals interactions. The accuracy of the method compared with experiments was 1.5 kJ.mol^{-1} of diamante or 5.71.10^{-4} a.u.

4.4. Chemometrics

The software R4Cal 4.1.14 Open Office STATISTICs for Windows 7 was used. The statistical significance was checked by a *t*-test. The model fit was determined by an F-test. ANOVA was also used [115–120]. The ProteoWizard 3.0.11565.0 (2017), mMass 5.0.0, QuanBrowser 2.0.7 (Thermo Fischer Scientific Inc. Massachusetts, USA), and AMDIS 2.71 (2012) software were utilized.

5. Conclusions

Results from the study provide empirical evidence for the following conclusions.

(A) In testing the capability of Equation (2) [$D_{SD}^{'',tot} = \sum_i^n D_{SD}^{'',i} = \sum_i^n 2.6388.10^{-17} \times \overline{I_i^2} - \left(\overline{I_i}\right)^2$]

to quantify the MS intensity of analyte ions with a short span of scan time, we contrasted the use of classical quantitative methods based on ICIS and trapezoidal integration algorithms of peak detection. The analysis of surfactants in biota via equation ln[D''_{SD}] = f(conc.) yields $|r| = 0.9999_1$ examining the peaks of BAC-C12 at m/z 212.209 $\pm$ 0.1 and 211.75 $\pm$ 0.15.

(B) Equation (4) [$\overline{I^{TOT,q}} = \frac{1}{2} \times \frac{A_I^q}{A_D^q} \times D_{SD}^{'',tot}$] has been proven for PARA ions. The relation between $\langle I \rangle_{exp}$ and $\langle I \rangle_{theor}$ shows $|r| = 0.9942_9$ and 0.96501.

(C) Parameter $|r| = 1$ has been obtained, determining the 3D molecular structures of PARA and its ions at m/z 152, 158, 174, 301, and 325 via the assessment of relation D''_{SD} = f(D_{QC}) in biota at CE = 25 V.

Abbreviations

ANOVA	Analysis of variance (chemometric method)
APCI	Atmospheric pressure chemical ionization (mass spectrometric method)
ATE	Atenolol
BAC-C12	Benzyl-dodecyl-dimethyl-ammonium chloride
BAC-C14	Benzyl-dimethyl-tetradecyl-ammonium chloride
BAC-C16	Benzyl-hexadecyl-dimethyl-ammonium chloride
BAC-C18	Benzyl-dimethyl-octadecyl-ammonium chloride
BOMD	Born-Oppenheimer molecular dynamics
CID	Collision-induced dissociation (mass spectrometric operation mode)
CE	Collision energy

DFT	Density functional theory (quantum chemical method)
DoF	Number of points–number of parameters
D_{QC}	Quantum chemical diffusion parameter according to Arrhenius's theory
D_{SD}, D_{SD}''	Stochastic dynamic diffusion parameters according to our theory
ESI	Electrospray ionization (mass spectrometric method)
FT-ICR	Fourier transform ion cyclotron resonance (mass spectrometric method)
GS	Ground state
IS	Internal standard
LMW	Low molecular weight (analyte)
MD	Molecular dynamics
MM	Molecular mechanics
MS	Mass spectrometry
MS/MS	Tandem mass spectrometric operation mode
PARA	Paracetamol
PES	Potential energy surface
PRO	Propranolol
QuEChERS	Quick, easy, cheap, effective, rugged, and safe (extraction method)
$\|r\|$	Statistical coefficient of linear correlation (chemometrics)
SD	Stochastic dynamics
SIM	Selected ion monitoring (mass spectrometric operation mode)
sd(yEr$\pm$)	Standard deviation (chemometrics)
SRM	Selected reaction monitoring (mass spectrometric operation mode)
se(yEr$\pm$)	Standard error (chemometrics)
TIA	Trapezoidal integration approach
TS	Transition state
ν_o^i	Frequencies at a stationary state of potential energy
ν_s^i	Frequency in a transition state of potential energy
$H^\#$	Activation enthalpy

References

1. Townsend, R. Mass spectrometric investigation of pharmaceuticals in environmental matrices: Homogenate analysis. Ph.D. Thesis, Swansea University, Swansea, UK, 2019. Available online: http://cronfa.swan.ac.uk/Record/cronfa50205 (accessed on 1 January 2019).

2. Gardner, M.; Comber, S.; Ellor, B. Summary of data from the UKWIR chemical investigations programme and a comparison of data from the past ten years' monitoring of effluent quality. *Sci. Total Environ.* **2022**, *832*, 155041. [CrossRef]

3. European Parliament and Council. Regulation (EU) No 528/2012 concerning the making available on the market and use of biocidal products. *Off. J. Eur. Union. L* **2012**, *167*, 1–122.

4. European Parliament and Council. Directive 2013/39/EU amending directives 2000/60/EC and 2008/105/EC as regards priority substances in the field of water policy. *Off. J. Eur. Commun Legis L* **2013**, *226*, 1–17.

5. Godfrey, A.; Dunscombe, J.; Gravell, A.; Hunter, A.; Barrow, M.; Van Keulen, G.; Desbrow, C.; Townsend, R. Use of QuEChERS as a manual and automated high-throughput protocol for investigating environmental matrices. *Chemosphere* **2022**, *308*, 136313. [CrossRef]

6. Townsend, R.; Van Keulen, G.; Desbrow, C.; Godfrey, A. An investigation of the utility of QuEChERS for extracting acid, base, neutral and amphiphilic species from example environmental and clinical matrices. *Anal. Sci. Adv.* **2020**, *1*, 152–160. [CrossRef]

7. Godfrey, A.; Townsend, R.; Desbrow, C.; Felion, C. QuEChERS: A simple extraction for monitoring quaternary ammonium biocide pollution in soils and antimicrobial resistance. *Anal. Met.* **2020**, *12*, 4387–4393. [CrossRef] [PubMed]

8. Paijens, C.; Bressy, A.; Frere, B.; Moilleron, R. Biocide emissions from building materials during wet weather: Identification of substances, mechanism of release and transfer to the aquatic environment. *Environ. Sci. Poll. Res.* **2020**, *2*, 3768–3791. [CrossRef] [PubMed]

9. Faccenda, H.; Melara, F.; Damini, G.; Godinho, M.; Manera, C.; Piccin, J. Graywater treatment of emerging pollutant linear alkylbenzene sulfonate by adsorption with leather shave waste activated carbon. *Environ. Sci. Poll. Res.* **2022**, *29*, 79830–79840. [CrossRef]

10. Yang, K.; Chen, M.; Zhua, D. Exposure to benzalkonium chloride disinfectants promotes antibiotic resistance in sewage sludge microbiomes. *Sci. Tot. Environ.* **2023**, *867*, 161527. [CrossRef]

11. Volcao, L.; Fraga, L.; De Lima Brum, R.; De Moura, R.; Bernardi, E.; Ramos, D.; Da Silva, L., Jr. Toxicity of biocide formulations in the soil to the gut community in balloniscus selowii Brandt, 1983 (Crustacea: Isopoda: Oniscidea). *Water Air Soil Poll.* **2020**, *231*, 306. [CrossRef]

12. Olkowska, E.; Polkowska, Z.; Namiesnik, I. Analytics of surfactants in the environment: Problems and challenges. *Chem. Rev.* **2011**, *111*, 5667–5700. [CrossRef] [PubMed]

13. UNESCO—United Nations Educational, Scientific, and Cultural Organization. Emerging Pollutants in Water and Wastewater. 2015. Available online: https://en.unesco.org/emergingpollutantsinwaterandwastewater#:~:text=These%20contaminants%20include%20mainly%20chemicals,surfactants%2C%20industrial%20additives%20and%20solvents (accessed on 1 June 2019).

14. Gray, M.; Peake, S.; Farrell, A.; Bruch, R. Acute didecyl dimethyl ammonium chloride toxicity to larval lake Sturgeon, Acipenser fulvescens Rafinesque, Walleye Sander vitreus Mitchill, and Northern Pike, Esox lucius Linnaeus. *Bull. Environ. Contam. Toxicol.* **2005**, *75*, 890–896. [CrossRef] [PubMed]

15. Gerba, C. Quaternary ammonium biocides: Efficacy in application. *Appl. Environ. Microbiol.* **2015**, *81*, 464–469. [CrossRef] [PubMed]

16. Tezel, U.; Tandukar, M.; Martinez, R.; Sobecky, P.; Pavlostathis, S. Aerobic biotransformation of n-tetradecylbenzyldimethyl ammonium chloride by an enriched *pseudomonas* spp. community. *Environ. Sci. Technol.* **2012**, *46*, 8714–8722. [CrossRef]

17. Liao, J.; Chen, Y. Removal of intl1 and associated antibiotics resistant genes in water, sewage sludge and livestock manure treatments. *Rev. Environ. Sci. Biotechnol.* **2018**, *17*, 471–500. [CrossRef]

18. Ajibola, A.; Zwiener, C. Occurrence and risk assessment of antibiotic residues in sewage sludge of two Nigerian hospital wastewater treatment plants. *Water Air Soil Poll.* **2022**, *233*, 405. [CrossRef]

19. Jansen, K.; Mohr, C.; Lügger, K.; Heller, C.; Siemens, J.; Mulder, I. Widespread occurrence of quaternary alkylammonium disinfectants in soils of Hesse, Germany. *Sci. Tot. Environ.* **2023**, *857*, 159228. [CrossRef]

20. Shackman, H.; Ding, W.; Bolgar, M. A novel route to recognizing quaternary ammonium cations using electrospray mass spectrometry. *J. Am. Soc. Mass Spectrom.* **2015**, *26*, 181–189. [CrossRef] [PubMed]

21. Ahmad, R.; Cho, E.; Rakhmat, S.; Hyun, M.; Park, C.; Kim, S. Characterization of structure isomers of ethylbenzalkyl dimethyl ammonium chlorides and quantification in commercial household disinfectant products. *Environ. Technol. Innov.* **2023**, *29*, 102979. [CrossRef]

22. Dew, N.; Bramer, T.; Edsman, K. Catanionic aggregates formed from drugs and lauric or capric acids enable prolonged release from gels. *J. Coll. Int. Sci.* **2008**, *323*, 386–394. [CrossRef]

23. Ertekin, E.; Hatt, J.; Konstantinidis, K.; Tezel, U. Similar microbial consortia and genes are involved in the biodegradation of benzalkonium chlorides in different environments. *Environ. Sci. Technol.* **2016**, *50*, 4304–4313. [CrossRef] [PubMed]

24. Ertekin, E.; Konstantinidis, K.; Tezel, U. A rieske-type oxygenase of *Pseudomonas sp.* BIOMIG1 converts benzalkonium chlorides to benzyldimethyl amine. *Environ. Sci. Technol.* **2017**, *51*, 175–181. [CrossRef] [PubMed]

25. Li, R.; Zhang, C.; Liu, D.; Sun, J. Biosorption of tetradecyl benzyl dimethyl ammonium chloride on activated sludge: Kinetic, thermodynamic and reaction mechanisms. *Biores. Technol.* **2011**, *102*, 3799–3804.

26. Zhang, C.; Tezel, U.; Li, K.; Liu, D.; Ren, R.; Du, J.; Pavlostathis, S. Evaluation and modeling of benzalkonium chloride inhibition and biodegradation in activated sludge. *Water Res* **2011**, *45*, 1238–1246. [CrossRef] [PubMed]

27. Berge, A.; Bulete, A.; Fildier, A.; Vulliet, E. High-resolution mass spectrometry as a tool to evaluate the sample preparation of sludge. *Anal. Chem.* **2017**, *89*, 9685–9694. [CrossRef] [PubMed]

28. Patrauchan, M.; Oriel, P. Degradation of benzyldimethylalkylammonium chloride by *aeromonas hydrophila sp.* K. *J. Appl. Microbiol.* **2003**, *94*, 266–272. [CrossRef]

29. Jia, Y.; Huang, Y.; Ma, J.; Zhang, S.; Liu, J.; Li, T.; Song, L. Toxicity of the disinfectant benzalkonium chloride (C14) towards cyanobacterium Microcystis results from its impact on the photosynthetic apparatus and cell metabolism. *J. Environ. Sci.* **2024**, *135*, 198–209. [CrossRef]

30. Ibusquiza, P.; Herrera, J.; Vázquez-Sanchez, D.; Parada, A.; Cabo, A. A new and efficient method to obtain benzalkonium chloride adapted cells of Listeria monocytogenes. *J. Microbiol. Meth.* **2012**, *91*, 57–61. [CrossRef] [PubMed]

31. Wang, Y.; Yang, Y.; Liu, X.; Zhao, J.; Liu, R.; Xing, B. Interaction of microplastics with antibiotics in aquatic environment: Distribution, adsorption, and toxicity. *Environ. Sci. Technol.* **2021**, *55*, 15579–15595. [CrossRef]

32. Li, W.; Zhang, X.; Han, J. Formation of larger molecular weight disinfection byproducts from acetaminophen in chlorine disinfection. *Environ. Sci. Technol.* **2022**, *56*, 16929–16939. [CrossRef]

33. Nejuma, K.; Manoj, P.; Aravind, U.; Aravindakumar, C. Sonochemical degradation of a pharmaceutical waste, atenolol, in aqueous medium. *Environ. Sci. Pollut. Res.* **2014**, *21*, 4297–4308. [CrossRef] [PubMed]

34. Bianchi, C.; Sacchi, B.; Pirola, C.; Demartin, F.; Cerrato, G.; Morandi, S.; Capucci, V. Aspirin and paracetamol removal using a commercialmicro-sized TiO_2 catalyst in deionized and tap water. *Environ. Sci. Pollut. Res.* **2017**, *24*, 12646–12654. [CrossRef] [PubMed]

35. Ahmed, F.; Tscharke, B.; O'Brien, J.; Hall, W.; Cabot, P.; Sowa, P.; Samanipour, S.; Thomas, K. National wastewater reconnaissance of analgesic consumption in Australia. *Environ. Sci. Technol.* **2023**, *57*, 1712–1720. [CrossRef] [PubMed]

36. Rouibah, I.; Hassen, W.; Sallem, O.; Khellaf, N.; Hassen, A.; Ben Mansour, H. Photocatalytic and biodegradation treatments of paracetamol: Investigation of the in vivo toxicity. *Environ. Sci. Poll. Res.* **2021**, *28*, 14530–14545. [CrossRef] [PubMed]

37. European Parliament and Council Directive of the European Parliament and of the Council establishing a framework for Community action in the field of water policy: 000/60/EC, 2008/105/EC, 2009/90/EC, 2013/39/EU, 2015/1787/EU. *Off. J. Eur. Union*. 2015. Available online: http://www.eur-lex.europa.eu/ (accessed on 6 October 2015).

38. Hall, L., Jr.; Bushong, S.; Ziegenfuss, M.; Johnson, W.; Herman, R.; Wright, D. Chromic toxicity of tributyltin to chesapeake bay biota. *Water Air Soil Poll.* **1988**, *39*, 365–376. [CrossRef]

39. Li, M.; Kwon, S.; Poulin, B.; Tsui, M.; Motta, L.; Cho, M. Internal dynamics and metabolism of mercury in biota: A review of insights from mercury stable isotopes. *Environ. Sci. Technol.* **2022**, *56*, 9182–9195. [CrossRef]

40. Couto, C.; Ribeiro, C. Pollution status and risk assessment of trace elements in Portuguese water, soils, sediments, and associated biota: A trend analysis from the 80s to 2021. *Environ. Sci. Poll. Res.* **2022**, *29*, 48057–48087. [CrossRef] [PubMed]

41. Figueiredo, C.; Oliveira, R.; Lopes, C.; Brito, P.; Caetano, M.; Raimundo, J. Rare earth elements biomonitoring using the mussel *Mytilus galloprovincialis* in the Portuguese coast: Seasonal variations. *Marine Poll. Bull.* **2022**, *175*, 113335. [CrossRef]

42. Saaibusquiza, S.; Herrara, J.; Cabo, M. Comparison between the resistance of benzalkonium chloride-adapted and nonadapted biofilms of Listeria monocytogenes to modified atmosphere packaging and nisin once transferred to mussels. *J. Food Prot.* **2011**, *74*, 1112–1118. [CrossRef]

43. Rosa, M.; Flores, Y.; Sierra, K.; Torres, B.; Ward, J. Examining effects of surfactants on particle clearance rate and capture efficiency of the blue mussel Mytilus edulis. *Aquat. Biol.* **2020**, *29*, 149–154. [CrossRef]

44. Donaher, S.; Dunn, R.; Gonzales, A.; Wattier, B.; Powell, B.; Martinez, N. Tissue-specific toxicokinetics of aqueous radium-226 in an estuarine mussel, *Geukensia demissa*. *Environ. Sci. Technol.* **2023**. [CrossRef]

45. Liu, F.; Ma, Z.; Deng, Y.; Wang, M.; Zhou, P.; Liu, W.; Guo, S.; Tong, M.; Ma, D. Tunable covalent organic frameworks with different heterocyclic nitrogen locations for efficient Cr(VI) reduction, Escherichia coli disinfection, and paracetamol degradation under visible-light irradiation. *Environ. Sci. Technol.* **2021**, *55*, 5371–5381. [CrossRef] [PubMed]

46. Zhang, H.; Jia, Y.; Khana, S.; Lu, H.; Fang, H.; Zhao, Q. Understanding the role of extracellular polymeric substances on ciprofloxacin adsorption in aerobic sludge, anaerobic sludge, and sulfate-reducing bacteria sludge systems. *Environ. Sci. Technol.* **2018**, *52*, 6476–6486. [CrossRef] [PubMed]

47. Prieto-Blanco, M.; Planas-Franco, A.; Muniategui-Lorenzo, S.; Gonzalez-Castro, M. Mixed-mode chromatography of mixed functionalized analytes as the homologues of benzalkonium chloride. Application to pharmaceutical formulations. *Talanta* **2023**, *255*, 124228. [CrossRef]

48. Pawar, A.; Mannepalli, C. Simple and validated stability indicating HPLC method for simultaneous quantification of brimonidine, timolol and benzalkonium chloride in anti-glaucoma ophthalmic formulations. *Asian J. Chem.* **2023**, *35*, 179–186. [CrossRef]

49. Pan, M.; Yau, P. Fate of macrolide antibiotics with different wastewater treatment technologies. *Water Air Soil Poll.* **2021**, *232*, 103. [CrossRef] [PubMed]

50. Alygizakis, N.; Samanipour, S.; Hollender, J.; Ibanez, M.; Kaserzon, S.; Kokkali, V.; Van Leerdam, J.; Mueller, J.; Pijnappels, M.; Reid, M.; et al. Exploring the potential of a global emerging contaminant early warning network through the use of retrospective suspect screening with high-resolution mass spectrometry. *Environ. Sci. Technol.* **2018**, *52*, 5135–5144. [CrossRef] [PubMed]

51. Xian, Y.; Dong, H.; Wu, Y.; Guo, G.; Hou, X.; Wang, B. QuEChERS-based purification method coupled to ultrahigh performance liquid chromatography-tandem mass spectrometry (UPLC–MS/MS) to determine six quaternary ammonium compounds (QACs) in dairy products. *Food Chem.* **2016**, *212*, 96–103. [CrossRef]

52. Dyshlyuk, L.; Fotina, N.; Milentyeva, L.; Ivanova, S.; Izgarysheva, N.; Golubtsova, Y. Antimicrobial and antioxidant activity of Panax ginseng and Hedysarum neglectum root crop extracts. *Brazilian J. Biol.* **2022**, *84*, e256944. [CrossRef]

53. Raesaenen, R.; Dwivedi, P.; Fernandez, F.; Kauppila, T. Desorption atmospheric pressure photoionization and direct analysis in real time coupled with travelling wave ion mobility mass spectrometry. *Rapid Commun. Mass Spectrom.* **2014**, *28*, 2325–2336. [CrossRef]

54. Zhang, M.; Lin, F.; Xu, J.; Xu, W. Membrane electrospray ionization for direct ultrasensitive biomarker quantitation in biofluids using mass spectrometry. *Anal. Chem.* **2015**, *87*, 3123–3128. [CrossRef] [PubMed]

55. Ivanova, B.; Spiteller, M. Stochastic dynamic mass spectrometric quantification of steroids in mixture—Part II. *Steroids* **2020**, *164*, 108750. [CrossRef] [PubMed]

56. Ivanova, B.; Spiteller, M. Stochastic dynamic mass spectrometric approach to quantify reserpine in solution. *Anal. Chem. Lett.* **2020**, *10*, 703–721. [CrossRef]

57. Chen, T.; Wu, M.; Chen, Y. Ultrasonication-assisted spray ionization-based micro-reactors for online monitoring of fast chemical reactions by mass spectrometry. *J Mass Spectrom.* **2019**, *54*, 26–34. [CrossRef] [PubMed]

58. Maus, A.; Kemp, J.; Hoffmann, T.; Ramsay, S.; Grebe, S. Isotopic distribution calibration for mass spectrometry. *Anal. Chem.* **2021**, *93*, 12532–12540. [CrossRef] [PubMed]

59. European Parliament and Council Directive of the European Parliament and of the Council Decision of 12 August 2002 implementing Council Directive 96/23/EC 18 concerning the performance of analytical methods and interpretation of results. *Off. J. 19 Eur. Commun. L* **2002**, *221*, 8–36.

60. Ivanova, B.; Spiteller, M. A stochastic dynamic mass spectrometric diffusion method and its application to 3D structural analysis of the analytes. *Rev. Anal. Chem.* **2019**, *38*, 1. [CrossRef]

61. Ivanova, B.; Spiteller, M. Mass spectrometric stochastic dynamic 3D structural analysis of mixture of steroids in solution—Experimental and theoretical study. *Steroids* **2022**, *181*, 109001. [CrossRef]

62. Ivanova, B.; Spiteller, M. Chapter 1: Mass spectrometric and quantum chemical treatments of molecular and ionic interactions of a flavonoid-O-glycoside—A stochastic dynamic approach. In *Advances in Chemistry Research*; Taylor, J., Ed.; NOVA Science Publishers: New York, NY, USA, 2022; Volume 74, pp. 1–126.

63. Ivanova, B.; Spiteller, M. Stochastic dynamic electrospray ionization mass spectrometric quantitative analysis of metronidazole in human urine. *Anal. Chem. Lett.* **2022**, *12*, 322–348. [CrossRef]

64. Ivanova, B.; Spiteller, M. Exact quantifying of mass spectrometric variable intensity of analyte peaks with respect to experimental conditions of measurements—A stochastic dynamic approach. *Anal. Chem. Lett.* **2022**, *12*, 542–561. [CrossRef]

65. Ivanova, B.; Spiteller, M. Stochastic dynamic ultraviolet photofragmentation and high collision energy dissociation mass spectrometric kinetics of triadimenol and sucralose. *Environ. Sci. Poll. Res.* **2022**. [CrossRef]

66. Ivanova, B.; Spiteller, M. Stochastic dynamic quantitative and 3D structural matrix assisted laser desorption/ionization mass spectrometric analyses of mixture of nucleosides. *J. Mol. Struct.* **2022**, *1260*, 132701. [CrossRef]

67. Ivanova, B.; Spiteller, M. Electrospray ionization stochastic dynamic mass spectrometric 3D structural analysis of Zn^{II}-ion containing complexes in solution. *Inorg. Nano-Met. Chem.* **2022**, *52*, 1407–1429. [CrossRef]

68. Baquer, G.; Sementé, L.; Mahamdi, T.; Correig, X.; Ràfols, P.; García-Altares, M. What are we imaging? Software tools and experimental strategies for annotation and identification of small molecules in mass spectrometry imaging. *Mass. Spec. Rev.* **2022**, e21794. [CrossRef] [PubMed]

69. Chen, H.; Zheng, J.; Zhang, X.; Luo, M.; Wang, Z.; Qiao, X. Surface desorption atmospheric pressure chemical ionization mass spectrometry for direct ambient sample analysis without toxic chemical contamination. *J. Mass Spectrom.* **2007**, *42*, 1045–1056. [CrossRef] [PubMed]

70. Gravel, A.; Guerette, C.; Fortin, D.; Auger, S.; Picard, P.; Segura, P. Further studies on the signal enhancement effect in laser diode thermal desorption-triple quadrupole mass spectrometry using microwell surface coatings. *J. Mass Spectrom.* **2019**, *54*, 948–956. [CrossRef]

71. Earnshaw, C.; Carolan, V.; Richards, D.; Clench, M. Direct analysis of pharmaceutical tablet formulations using matrix-assisted laser desorption/ionisation mass spectrometry imaging. *Rapid Commun. Mass Spectrom.* **2010**, *24*, 1665–1672. [CrossRef]

72. Ostrowski, W.; Karczewska, K.; Frański, R. Oxidation of paracetamol by Cu^{2+}-formation of the paracetamol radical cation. *Rapid Commun. Mass Spectrom.* **2013**, *27*, 1579–1584. [CrossRef]

73. Yao, Y.; Wu, L.; Sun, W.; Luo, Z.; Di, D.; Yuan, Z.; Huang, Z.; Hu, B. Fast-switching high-voltage porous-tip electrospray ionization mass spectrometry for rapid detection of antirheumatic drugs in adulterated herbal dietary supplements. *Rapid Commun. Mass. Spectrom.* **2019**, *33*, 1877–1883. [CrossRef]

74. Chan, C.; Bolgar, M.; Miller, S.; Attygalle, A. A combined desorption ionization by charge exchange (DICE) and desorption electrospray onization (DESI) source for mass spectrometry. *J. Am. Soc. Mass Spectrom.* **2011**, *22*, 173–178. [CrossRef]

75. Winter, G.; Wilhide, J.; LaCourse, W. Molecular ionization-desorption analysis source (MIDAS) for mass spectrometry: Thin-layer chromatography. *J. Am. Soc. Mass Spectrom.* **2016**, *27*, 352–358. [CrossRef] [PubMed]

76. Lu, W.; Zhao, S.; Gong, M.; Sun, L.; Ding, L. Simultaneous determination of acetaminophen and oxycodone in human plasma by LC-MS/MS and its application to a pharmacokinetic study. *J. Pharmaceut. Anal.* **2018**, *8*, 160–167. [CrossRef]

77. Belal, T.; Awad, T.; Clark, C. Determination of paracetamol and tramadol hydrochloride in pharmaceutical mixture using HPLC and GC-MS. *J. Chromatogr. Sci.* **2009**, *47*, 849–854. [CrossRef] [PubMed]

78. Schaefermann, S.; Hauk, C.; Wemakor, E.; Neci, R.; Mutombo, G.; Ndze, E.; Cletus, T.; Nyaah, F.; Pattinora, M.; Wistuba, D.; et al. Substandard and falsified antibiotics and medicines against noncommunicable diseases in western Cameroon and Northeastern Democratic Republic of Congo. *Am. J. Trop. Med. Hyg.* **2020**, 1–15. [CrossRef] [PubMed]

79. Gilpin, R.; Zhou, W. Studies of the thermal degradation of acetaminophen using a conventional HPLC approach and electrospray ionization-mass spectrometry. *J. Chromatogr. Sci.* **2004**, *42*, 15–20. [CrossRef]

80. Upthagrove, A.; Hackett, M.; Nelson, W. Fragmentation pathways of selectively labeled uropranolol using electrospray ionization on an ion trap mass spectrometer and comparison with ions formed by electron impact. *Rapid Commun. Mass Spectrom.* **1999**, *13*, 534–541. [CrossRef]

81. Conte, J., Jr.; Lin, E.; Zhao, Y.; Zurlinden, E. A high-pressure liquid chromatographic-tandem mass spectrometric method for the determination of ethambutol in human plasma, bronchoalveolar lavage fluid, and alveolar cells. *J. Chromatogr. Sci.* **2002**, *40*, 113–118. [CrossRef]

82. Li, D.; Sheng, L.; Liu, X.; Yang, S.; Liu, Z.; Li, Y. Determination of TBI-166, a novel antituberculotic, in rat plasma by liquid chromatography-tandem mass spectrometry. *Chromatographia* **2014**, *77*, 1697–1703. [CrossRef]

83. He, H.; Li, L.; Zhao, L.; Sun, N.; Zhang, M.; Cheng, Y.; Yu, L.; Ma, L.; Wang, X. An improved HPLC-MS/MS method for simultaneous quantification of propranolol and its two phase I metabolites in plasma of infants with hemangioma and its application to a comparative study of plasma concentrations. *RSC Adv.* **2018**, *8*, 37286–37294. [CrossRef]

84. Johnson, R.; Lewis, R. Quantitation of atenolol, metoprolol, and propranolol in postmortem human fluid and tissue specimens via LC/APCI-MS. *Forensic. Sci. Int.* **2006**, *156*, 106–117. [CrossRef]

85. Cahill, J.; Kertesz, V.; Weiskittel, T.; Vavrek, M.; Freddo, C.; Van Berkel, G. Online, absolute quantitation of propranolol from spatially distinct 20- and 40-μm dissections of brain, liver, and kidney thin tissue sections by laser microdissection-liquid vortex capture-mass spectrometry. *Anal. Chem.* **2016**, *88*, 6026–6034. [CrossRef] [PubMed]

86. Rix, M.; Webstar, B. Electron impact-induced eliminations of acetaldehyde. *J. Chem. Soc. B* **1968**, 254–258. [CrossRef]

87. Svan, A.; Hedeland, M.; Arvidsson, T.; Jasper, J.; Sedlakd, D.; Petterssona, C. Identification of transformation products from β-blocking agents formed in wetland microcosms using LC-Q-ToF. *J. Mass Spectrom.* **2016**, *51*, 207–218. [CrossRef] [PubMed]

88. Jeong, E.; Kim, S.; Cha, E.; Lee, K.; Kim, H.; Lee, S.; Kwon, O.; Lee, J. Simultaneous analysis of 210 prohibited substances in human urine by ultrafast liquid chromatography/tandem mass spectrometry in doping control. *Rapid Commun. Mass Spectrom.* **2015**, *29*, 367–384. [CrossRef]

89. Huang, G.; Li, G.; Cooks, R. Induced nanoelectrospray ionization for matrix-tolerant and high-throughput mass spectrometry. *Angew. Chem. Int. Ed.* **2011**, *50*, 9907–9910. [CrossRef]

90. Parson, W.; Schneider, B.; Kertesz, V.; Corr, J.; Covey, T.; Van Berkel, G. Rapid analysis of isomeric exogenous metabolites by differential mobility spectrometry—Mass spectrometry. *Rapid Commun. Mass Spectrom.* **2011**, *25*, 3382–3386. [CrossRef]

91. Salomonsson, M.; Bondessona, U.; Hedelanda, M. In vitro formation of phase I and II metabolites of propranolol and determination of their structures using chemical derivatization and liquid chromatography-tandemmass spectrometry. *J. Mass. Spectrom.* **2009**, *44*, 742–755. [CrossRef]

92. Vonaparti, A.; Lyris, E.; Angelis, Y.; Panderi, I.; Koupparis, K.; Tsantili-Kakoulidou, A.; Peters, R.; Nielen, M.; Georgakopoulos, C. Preventive doping control screening analysis of prohibited substances in human urine using rapid-resolution liquid chromatography/high-resolution time-of-flight mass spectrometry. *Rapid Commun. Mass Spectrom.* **2010**, *24*, 1595–1609. [CrossRef]

93. Shariatgorji, M.; Amini, N.; Thorsen, G.; Crescenzi, G.; Ilag, L. μ-Trap for the SALDI-MS screening of organic compounds prior to LC/MS analysis. *Anal. Chem.* **2008**, *80*, 5515–5523. [CrossRef]

94. Gergov, M.; Robson, J.; Duchoslav, E.; Ojanpera, L. Automated liquid chromatographic/tandem mass spectrometric method for screening β-blocking drugs in urine. *J. Mass Spectrom.* **2000**, *35*, 912–918. [CrossRef]

95. Yoneda, M.; Tsujimoto, K.; Ohashi, M.; Shiratsuchi, M.; Ohkawa, Y. Structures of [M-44]$^+$ ions in the electron impact and fast atom bombardment mass spectra of the β-blocker nipradilol with a nitrate ester group. *Org. Mass Spectrom.* **1990**, *25*, 146–150. [CrossRef]

96. Tay, K.; Rahman, N.; Abas, M. Characterization of atenolol transformation products in ozonation by using rapid resolution high-performance liquid chromatography/quadrupole-time-of-flight mass spectrometry. *Microchem. J.* **2011**, *99*, 312–326. [CrossRef]

97. Kumar, V.; Shah, R.; Malik, S.; Singh, S. Compatibility of atenolol with excipients: LC-MS/TOF characterization of degradation/interaction products, and mechanisms of their formation. *J. Pharmaceut. Biomed. Anal.* **2009**, *49*, 880–888. [CrossRef] [PubMed]

98. Hou, K.; Xu, W.; Xu, J.; Cooks, R.; Ouyang, Z. Sampling wand for an ion trap mass spectrometer. *Anal. Chem.* **2011**, *83*, 1857–1861. [CrossRef] [PubMed]

99. Aksenova, L.; Koval, V.; Chernonosov, A. Parallel reaction monitoring mode for atenolol quantification in dried plasma spots by liquid chromatography coupled with high-resolution mass spectrometry. *Processes* **2022**, *10*, 1240. [CrossRef]

100. Medana, C.; Calza, P.; Carbone, F.; Pelizzetti, E.; Hidaka, H.; Baiocchi, C. Characterization of atenolol transformation products on light-activated TiO$_2$ surface by high-performance liquid chromatography/high-resolution mass spectrometry. *Rapid Commun. Mass Spectrom.* **2008**, *22*, 301–313. [CrossRef] [PubMed]

101. Townsend, R.; Godfrey, A.; Van Keulen, G.; Geertje, A.; Brenton, G. *Mass Spectrometric Investigation of Pharmaceuticals in Environmental Matrices—Homogenate Analysis: Thesis Data 1*; Zenodo: Geneva, Switzerland; p. 2022. [CrossRef]

102. Townsend, R.; Godfrey, A.; Van Keulen, G.; Geertje, G. *Mass Spectrometric Investigation of Pharmaceuticals in Environmental Matrices—Homogenate Analysis: Thesis Data 2*; Zenodo: Geneva, Switzerland, 2022. [CrossRef]

103. Ferrera, I.; Furlong, E. Identification of alkyl dimethyl benzylammonium surfactants in water samples by solid-phase extraction followed by ion trap LC/MS and LC/MS/M. *Environ. Sci. Technol.* **2001**, *35*, 2583–2588. [CrossRef] [PubMed]

104. Xia, Y.; Lau, J.; Olah, T.; Jemal, M. Targeted quantitative bioanalysis in plasma using liquid chromatography/high-resolution accurate mass spectrometry: An evaluation of global selectivity as a function of mass resolving power and extraction window, with comparison of centroid and profile modes. *Rapid Commun. Mass Spectrom.* **2011**, *25*, 2863–2878.

105. Zeng, J.; Tao, Y.; Giese, T.; York, D. QDπ: A quantum deep potential interaction model for drug discovery. *J. Chem. Theory Comput.* **2023**, *19*, 1261–1275. [CrossRef]

106. Brown, D. *The Chemical Bond in Inorganic Chemistry*; Oxford University Press: Oxford, UK, 2002; pp. 1–279.

107. Bader, R.; Nguyen-Dang, T.; Tal, Y. A topological theory of molecular structure. *Rep. Prog. Phys.* **1981**, *44*, 894–948. [CrossRef]

108. Zacs, D.; Bartkevics, V. Trace determination of perfluorooctane sulfonate andperfluorooctanoic acid in environmental samples (surface water, wastewater, biota, sediments, and sewage sludge) using liquidchromatography—Orbitrap mass spectrometry. *J. Chromatogr. A* **2016**, *1473*, 109–121. [CrossRef] [PubMed]

109. Frisch, M.; Trucks, G.; Schlegel, H.; Scuseria, G.; Robb, M.; Cheeseman, J.; Fox, D. Gaussian 09, 98; Pittsburgh, Wallingford CT; Gaussian, Inc.: 1998, 2009. Available online: www.gaussian.com (accessed on 1 January 2016).

110. Helgaker, T.; Jensen, H.; Jrgensen, P.; Olsen, J.; Ruud, K.L.; Agren, H.; Auer, A.; Bak, K.; Bakken, V.; Christiansen, O.; et al. Dalton Program Package. 2011. Available online: http://www.daltonprogram.org/download.html (accessed on 1 January 2011).

111. Gordon, M.; Schmidt, M. Advances in Electronic Structure Theory: GAMESS a Decade Later. In *Theory and Applications of Computational Chemistry: The First Forty Years*; Dykstra, C., Frenking, G., Kim, K., Scuseria, G., Eds.; Elsevier: Amsterdam, The Netherlands, 2005; pp. 1167–1189.

112. Nielsen, A.; Holder, A. *Gauss View 5.0, User's Reference. Pittsburgh GausView03 Program Package*; GAUSSIAN Inc.: Wallingford, CT, USA, 2009; Available online: www.gaussian.com/g_prod/gv5.htm (accessed on 1 January 2009).

113. Burkert, U.; Allinger, A. *Molecular Mechanics in ACS Monograph 177*; American Chemical Society: Washington, DC, USA, 1982; pp. 1–339.

114. Allinger, L. Conformational analysis. 130. MM2. A hydrocarbon force field utilizing V1 and V2 torsional terms. *J. Am. Chem. Soc.* **1977**, *99*, 8127–8134. [CrossRef]

115. Kelley, C. Iterative Methods for Optimization. In *Society for Industrial and Applied Mathematics*; SIAM: Philadelphia, PA, USA, 2009; p. 18.

116. Otto, M. *Chemometrics*, 3rd ed.; Wiley: Weinheim, Germany, 2017; pp. 1–383.

117. Apache OpenOffice. Available online: http://de.openoffice.org (accessed on 1 January 2023).

118. Madsen, K.; Nielsen, H.; Tingleff, T. *Informatics and Mathematical Modelling*, 2nd ed.; DTU Press: Kongens Lyngby, Denmark, 2004.

119. Miller, J.; Miller, J. *Statistics and Chemometrics for Analytical Chemistry*; Pentice Hall: London, UK, 1988; pp. 1–271.

120. Taylor, J. *Quality Assurance of Chemical Measurements*; Lewis Publishers, Inc.: Boca Raton, FL, USA, 1987; pp. 1–328.